Original Research Article

Structure activity relationship, topological analysis and molecular docking analysis of pharmaceutical molecule 2356 -Tetrafluoro-4-pyridine carbonitrile

ABSTRACT

The theoretical vibrational spectral features of 2,3,5,6 Tetrafluoro-4-pyridinecarbonitrile were explored and compared with experimental results. The geometrical parameters, vibrational wavenumbers, bonding features and Energies were calculated at the B3LYP level with the basis set 6-311++G(d,p) levels. The calculated wavenumbers, vibrational energy distribution Analysis (VEDA), potential energy distributions (PEDs), and vibrational spectra were used to suggest reliable vibrational assignments. Molecular Electrostatic Potential investigations revealed the reactive zones around the molecule. The computed HOMO-LUMO energies were -8.369 and -3.380 eV, respectively, indicating charge transfer inside the molecule. The charge transfer of charge due to intra molecule interactions has been explained using natural bond orbital analysis. The ELF and LOL calculations were provide a visual aid for interpreting the results of electronic structure. The molecular docking approach was used to find the optimal ligand–protein orientation using the ligand 2,3,5,6 Tetrafluoro-4-pyridinecarbonitrile, which was docked with five distinct proteins. The main aim of the present study is to evaluate the biological activity of the selected compound using theoretical calculations

***Keywords*:** Natural Bond Orbital, Reduced Density Gradient (RDG). Fukui Function, MEP, VEDA.

1.Introduction

Pyridine is a heterocyclic chemical molecule that structurally similar to benzene but has a nitrogen atom in place of the C–H linkage. It is extremely useful since it is utilized in the production of a variety of organic products, medicines, medications, and agrochemical compounds. Antimicrobial (antifungal and antibacterial) and anticancer activities are also found in pyridine and pyridine derivatives. Pyridine is a highly stable chemical with a strong aromatic flavour. The pyridine ring structure is found in a wide variety of compounds in nature. Vitamin B6 and nicotinamide adenine are two such examples. In the biochemical and pharmaceutical industries, there is a lot of attention. Because of its higher polarity, the pyridine system allows greater intermolecular interaction. The nitrogen lone pair is found in a sp^2-hybridised orbital perpendicular to the ring's π-system. Most pyridines' ring nitrogen undergoes protonation, acylation and alkylation processes [1-6]. Anesthetics, medications for specific

brain illnesses, and pro-drugs for repairing neuronal damage induced by stroke are all treated with pyridine derivatives [7]. Insecticides, herbicides, fungicides, enzyme inhibitors and plant growth regulators are just a handful of good applications for pyridine-like compounds in agriculture [8]. The title compound contains substituted pyridine and cyano (carbonitrile) group attached to the compound. These cyanopyridine derivatives play an essential role in organic chemistry, as well as medicine and pharmacology, because they have anticancer, antiarrhythmic, anticonvulsant, antiparkinsonian, and antibacterial properties [9-11]. The implementation of various groups or rings into the pyridine structure results in diverse biochemical behaviour and biological activity. Antimicrobial, cardiovascular, antihypertensive, analgesic, antipyretic, anti-inflammatory and 1KK-β inhibitor activities have been discovered in cyanopyridines with various alkyl and aryl groups [12].

Density functional theory (DFT) is a widely used method for calculating molecular structures, vibrational frequencies, and energy. DFT calculations using the hybrid exchange-correlation functional B3LYP (Becke's three (B3) parameter exchange in combination with the Lee–Yang–(LYP) Parr's correlation functional) have been shown to be more effective and exhibit great accord with experimental values of structural features of pyridine and its derivatives than estimations using the gradient corrected exchange functional. The Mulliken atomic charge distribution and molecular electrostatic potential surface map were plotted using DFT studies with B3LYP as the basic set parameter. The first-order hyperpolarizability was determined. NBO calculations were carried out with the NBO 3.1 software, which was included with Gaussian 09. The FMOs were predicted and Koopman's theorem was used to compute parameters such as ionization energy, electron affinity, chemical potential, global hardness, and electrophilicity for the molecule. The vibrational modes were allocated using the VEDA software program on the basis of potential energy distribution (PED) calculations. Additionally, using the Localized Orbital Locator (LOL), Electron Localization Function (ELF) and Reduced Density Gradient (RDG) chemically interacting areas in the molecule have been investigated. Docking studies (for protein-ligand binding) have also been published to understand the biological activity of the selected compound.

2. Computational Details:

The density functional theory (DFT/B3LYP) at the 6-311++G(d,p) set level was used to calculate the optimized parameters and vibrational wavenumbers of the normal modes of the 2356-Tetrafluoro-4-pyridine carbonitrile (2356TF4PC) molecule. All the theoretical calculations were

performed using the Gaussian 09 W program package [13] with the default convergence criteria, without any constraint on the geometry [14]. The equilibrium geometry corresponding with the true minimum on the potential energy surface (PES) was effectively obtained by solving self-consistent field equation. The vibrational spectra of the 3ES were obtained by taking the second derivative of the energy, computed analytically. The optimized structural parameters were used in the vibrational frequency calculations at DFT levels to characterize all stationary points as minima using the GAUSSVIEW animation program [15]. By the use of total energy distribution (TED) using VEDA 4 program [16] along with available related molecules, the vibrational assignments were made with a high degree of accuracy. The harmonic vibrational wavenumbers have been analytically calculated by taking the second- order derivative of energy using the similar level theory. The calculated vibrational wavenumber was scaled down by using the scaling factor [17] for the B3LYP/6-31G(d) and B3LYP/6-311++G(d,p) level to offset the systematic error caused by neglecting anharmonicity and electron density. The Raman activities (Si) calculated with Gaussian '09 program converted to relative Raman intensities (Ii) using the following relationship derived from the intensity theory of Raman scattering [18] given by Eqn. (1) as:

$$I_i = \frac{f(\nu_o - \nu_i)^4 S_i}{\nu_i\left[1 - \exp\left(\frac{-hc\nu_i}{kT}\right)\right]} \qquad (1)$$

where ν_0 is the exciting wavenumber, ni is the vibrational wavenumber of the ith normal mode, h, c, and k are universal constants, and 'f ' is a suitably chosen common scaling factor for all the peak intensities. The simulated IR and Raman spectra were plotted using pure Lorentzian band shapes with a FWHM of 10 cm^{-1}. The Natural Bond Orbital (NBO) calculations were performed using NBO 5.1 program [20] as implemented in the Gaussian 09W [13] package at the DFT/B3LYP level. The Electron Localization Function (ELF), Localized Orbital Locator (LOL), Fukui function, and RDG were calculated using Multiwfn. The vibrational frequencies were determined using Vibrational energy Distribution Analysis (VEDA) software. Auto dock vina software was used to conduct molecular docking investigations to study the biological activities of the selected compound.

3. Result and conclusion:

3.1 Molecular Geometry:

B3LYP/6-311++G[d,p] level in DFT theory has improved the 2,3,5,6 Tetrafluoro-4-pyridinecarbonitrile (2356TF4PC) in order to obtain fundamental structural parameters such as

bond length, bond angle and dihedral angle. The most optimal lattice parameters namely bond length, bond angle and dihedral angle were derived for twelve atoms of 2356TF4PC produced from Gaussian 09W software program and their values are reported in Table (1). The optimised structure of the title compound is shown in fig (1). The aromatic ring contains solely carbon and nitrogen atoms, and their properties vary owing to chain lengths, branched chains and bond type.

The theoretical values of carbon-carbon single bond lengths of C_2-C_3, C_3-C_4, C_4-C_5 and C_5-C_6 are 1.391 Å, 1.399 Å, 1.399 Å and 1.391 Å which are nearly equal to the normal C-C bond length, while the carbon atom C_4-C_9 bond length is 1.425 much higher than other C-C bond lengths. This is due to the electronegative nitrogen atom N_{10} attached to the C_9 carbon atom. The theoretical bond lengths of carbon and fluorine of C_2-F_7, C_3-F_8, C_5-F_{11} and C_6-F_{12} are 1.329 Å, 1.330 Å, 1.330 Å and 1.329 Å lesser than the normal C-F bond length 1.35 Å. The interaction between C≡N is indicated by the decrease in endocyclic angles of C_2-C_3-C_4 (118.5^o), C_3-C_4-C_5 (117.6^o), and C_4-C_5-C_6 (118.5^o). The increased endocyclic angle of N_1-C_2-C_3 (124.7^o) indicates the presence of a highly electronegative nitrogen atom N1 inside the ring.

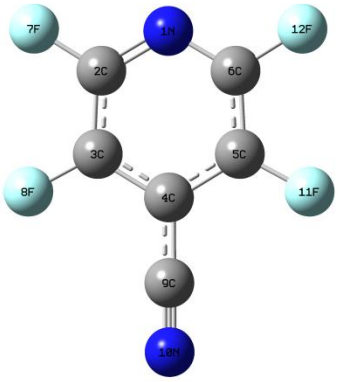

Figure 1: Optimized structure of 2356TF4PC molecule

Table 1: Optimized geometric parameters of 2,3,5,6 Tetrafluoro-4-pyridine carbonitrile molecule

Bond length	Value (Å)	Bond Angle	Value(^{o})	Dihedral Angle	Value(^{o})
N_1-C_2	1.310	N_1-C_2-C_3	123.2	N_1-C_2-C_3-C_4	0.0
C_2-C_3	1.391	C_3-C_2-F_7	119.0	F_7-C_2-C_3-C_4	180.0
C_2-F_7	1.329	C_2-C_3-C_4	118.5	C_2-C_3-C_4-C_5	0.0
C_3-C_4	1.399	C_4-C_3-F_8	120.6	C_2-C_3-C_4-C_9	180.0
C_3-F_8	1.330	C_3-C_4-C_5	117.6	F_8-C_3-C_4-C_5	180.0

C_4-C_5	1.399	C_3-C_4-C_9	121.2	C_3-C_4-C_5-C_6	0.0
C_4-C_9	1.425	C_4-C_5-C_6	118.5	C_3-C_4-C_5-F_{11}	180.0
C_5-C_6	1.391	C_4-C_5-F_{11}	120.6	C_4-C_5-C_6-F_{12}	180.0
C_5-F_{11}	1.330	C_5-C_6-F_{12}	119.0		
C_6-F_{12}	1.329	C_4-C_9-N_{10}	180.0		
C_9-N_{10}	1.153				

3.2 Natural Bond Orbital Analysis:

NBO analysis provides the most accurate possible 'natural Lewis structure', because all orbital details are mathematically chosen to include the highest possible percentage of the electron density. A useful aspect of the NBO method is that it gives information about interactions in both filled and virtual orbital spaces that could enhance the analysis of intra- and intermolecular interactions. The second order Fock matrix was carried out to evaluate the donor–acceptor interactions in the NBO analysis. The NBOs are helpful because they provide an accurate approach for analysing intramolecular and intermolecular bonding and interaction among bonds, as well as a solid foundation for exploring charge transfer and conjugative interaction in many molecular systems. Because all orbitals are mathematically selected to incorporate the largest possible percentage of the electron density, NBOs provide the most convenient 'natural Lewis structure' representation of ψ [21]. To investigate various second-order interactions in the molecular system, the natural bond orbital (NBO) calculations were done using the NBO 3.1 program implemented in Gaussian 09 software and the key results are summarised in Table (2).

Table 2: Second order perturbation theory analysis of Fock matrix in Natural Bond of 2,3,5,6 Tetrafluoro-4-pyridine carbonitrile molecule

Donor (i)	ED(e)	Acceptor (j)	ED(e)	E(2)[a] (Kcal/mol)	E(i)-E(j)[b] a.u	F(i.j)[c] a.u
π(N_1-C_6)	1.7373	π*(C_2-C_3)	0.3907	26.33	0.33	0.061
		π*(C_4-C_5)	0.4458	12.97	1.43	0.026
π(C_2-C_3)	1.6150	π*(N_1-C_6)	0.4565	18.63	0.28	0.066
		π*(C_4-C_5)	0.4458	22.01	0.29	0.072
π(C_4-C_5)	1.6668	π*(N_1-C_6)	0.4565	24.84	0.28	0.076
		π*(C_2-C_3)	0.3907	18.31	0.29	0.065
σ(C_4-C_9)	1.9783	σ*(C_9-N_{10})	0.0099	8.12	1.68	0.105
σ(C_9-N_{10})	1.9941	σ*(C_4-C_9)	0.0280	7.72	1.54	0.098

$LP1N_1$	1.8612	$\sigma^*(C_2\text{-}C_3)$	0.0472	8.30	0.87	0.078
		$\sigma^*(C_2\text{-}F_7)$	0.0557	7.84	0.64	0.065
		$\sigma^*(C_5\text{-}C_6)$	0.0472	8.30	0.87	0.078
		$\sigma^*(C_6\text{-}F_{12})$	0.0557	7.84	0.64	0.065
$LP1N_{10}$	1.9728	$\sigma^*(C_4\text{-}C_9)$	0.0280	11.17	1.00	0.094

According to the second-order perturbation theory analysis of Fock-matrix in NBO basis, strong intra-molecular hyperconjugative interactions are formed by orbital overlap between $\pi(N_1–C_6) \rightarrow \pi^*(C_2–C_3)$ and $\pi(C_4–C_5) \rightarrow \pi^*(N_1–C_6)$ bond orbitals with stabilization energies 26.33 kJ mol^{-1}, 24.84 kJ mol^{-1} resulting in intra-molecular charge transfer and system stabilisation. The intramolecular hyper conjugation interaction of the σ and π electrons of C-C to the anti C-N and C-N to anti C-C bond in the ring leads to the stability of specific parts of the ring, as seen in Table (2). The large value of E(2) indicates that the interaction between electron donors and electron acceptors is more intense, i.e., larger electrons are donated from electron donors to electron acceptors and the larger the extent of conjugation of the entire system [22]. The intra-molecular hyper conjugative interaction of LP_1 $(N_1) \rightarrow \sigma^*$ $(C_2– C_3)$ and LP_1 $(N_{10}) \rightarrow \sigma^*$ $(C_4–C_9)$ shows higher stabilization energies of 8.30 kJ mol^{-1} and 11.17 kJ mol^{-1} with increasing electron density 1.00e decreases the bond of $C_4–C_9$.

3.3 HOMO-LUMO Energy Analysis

HOMO-LUMO Analysis is also known as Frontier Molecular Orbital Analysis (FMOs). Many cyanopyridine derivatives have anticancer and antimicrobial properties, and calculations of key descriptors are crucial for determining the exact nature of interactions with electrophones and nucleophiles, as well as predicting the behaviour of these derivatives. The HOMO and LUMO orbitals, energy band gap (ΔE_g), electro negativity (χ), chemical potential (μ), global hardness (η), Ionisation potential (IP), global softness (S), electron affinity (EA) and global electrophilicity index (ω) descriptors are used for these derivatives. And these descriptors give more information regarding the discovery of new drugs [23,24].

$$\Delta E_g = E_{HOMO} - E_{LUMO}$$

$$IP = -E_{HOMO}$$

$$EA = -E_{LUMO}$$

$$\chi = -1/2(E_{LUMO} + E_{HOMO})$$

$$\mu = 1/2(E_{LUMO} + E_{HOMO})$$

$$\eta = 1/2(E_{LUMO} - E_{HOMO})$$

$$S = 1/2\eta$$

$$\omega = \mu^2/2\eta$$

The calculated HOMO-LUMO energy values and other global parameters are given in table (3) and the HOMO-LUMO structure for the title compound is shown in fig (2). FMOs indicate a molecule's structural stability as well as its kinetic stability and chemical reactivity. Furthermore, the FMOs aid in the prediction of a molecule's most reactive site [25]. The HOMO-LUMO energy gap of the title compound is 4.989eV. If the HOMO-LUMO energy gap is small, then the biological activity, chemical reactivity and polarizability of the compound are higher. Similarly, if the HOMO-LUMO energy gap is larger, the chemical reactivity, polarizability and biological activity of the compound are smaller. Thus, it is proved that the title compound has more biological activity.

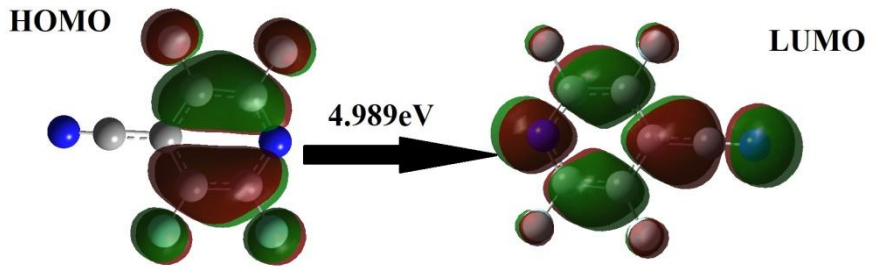

Figure 2: HOMO-LUMO energy gap of 2356TF4PC molecule

Table 3: Global reactivity descriptors of 2,3,5,6 Tetrafluoro-4-pyridine carbonitrile molecule

Molecular Properties	Mathematical Description	Energy(eV)
E_{HOMO}	Energy of HOMO	-8.369
E_{LUMO}	Energy of LUMO	-3.380
Energy Gap	$\Delta E_g = E_{HOMO} - E_{LUMO}$	4.989
Ionization Potential(IP)	$IP = -E_{HOMO}$	8.369
Electron Affinity (EA)	$EA = -E_{LUMO}$	3.380
Electronegativity (χ)	$\chi = -1/2(E_{LUMO} + E_{HOMO})$	5.875
Chemical potential (μ)	$\mu = 1/2(E_{LUMO} + E_{HOMO})$	-5.875

Global Hardness(η)	$\eta = 1/2(E_{LUMO} - E_{HOMO})$	2.495
Softness (S)	$S = 1/2\eta$	0.200
Electrophilicity index (ω)	$\omega = \mu^2/2\eta$	6.918

3.4 Molecular Electrostatic potential

DFT calculations with the optimised structure and B3LYP/6-31G(d,p) basis set were used to determine the compound's MEP surface analysis. The molecular electrostatic potential (MEP) is a tool for predicting nucleophilic and electrophilic attack locations in a molecule. The molecular electrostatic potential (MEP) is a valuable descriptor for understanding hydrogen-bonding interactions and is connected to the electronic density [26,27]. Electrophilic reactivity was linked to the negative (red) areas of MEP, while nucleophilic reactivity was linked to the positive (blue) portions. The solid, mesh and transparent surfaced molecular electrostatic potential of the given compound is shown in fig (3).

The distribution of charges in a molecule can be shown using molecular electrostatic potential maps. It's also utilised to predict the size and shape of the molecule. The formula ‘Force x distance' is used to compute electrostatic energy. The dipole moment, partial charges, electro negativity and chemical reactivity site of the molecule are all related to electrostatic potential. It provides a visual representation of a molecule's relative polarity. The map's colour code ranges from $-8.342e^{-2}$ to $8.342e^{-2}$. The lowest electro static potential energy is represented by the red colour, while the greatest value is represented by the blue colour. The negative electrostatic potential is associated with an attraction of the proton by the molecule's concentrated electron density. In regions where electron density is low and the nuclear charge is incompletely insulated, the positive electrostatic potential

correlates to proton repulsion by atomic nuclei. The blue colour in MEP is around the hydrogen atom and the red colour is around the nitrogen atom, highly electronegative atom.

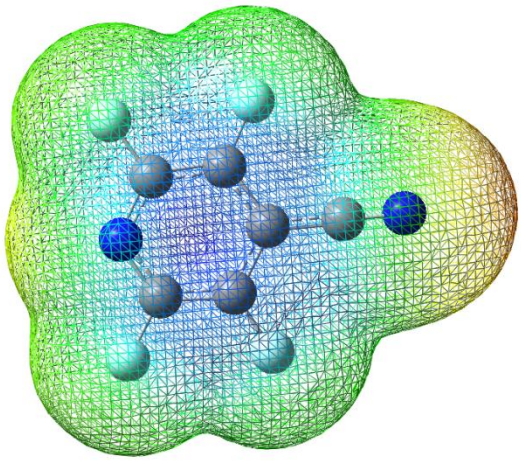

Figure 3: Molecular Electrostatic Potential colour filled map of 2356TF4PC molecule

3.5 Mulliken Population Analysis

Mulliken population analysis was used to determine the atomic charge values. The Mulliken atomic charges are calculated using the basis function to determine the electron population of each atom. The electrical charge on the chelating atoms determines a molecule's bonding capacity. Mulliken atomic charge computation is significant in the application of quantum chemical calculations to molecular systems, because atomic charges influence dipole moment, molecule polarizability, electronic structure, and many other aspects of molecular systems [28-29]. Mulliken atomic charge calculated at B3LYP/6-311++ level is represented in table (4) and the charge distribution of 2356TF4PC is shown in fig (4).

Table 4: Calculated Natural Charge of 2,3,5,6 Tetrafluoro-4-pyridine carbonitrile molecule

S.No	Atom	Mulliken Atomic Charge	Natural Charge
1.	N	-0.126659	-0.45405
2.	C	0.193832	0.56037
3.	C	-0.218231	0.37312
4.	C	1.841352	-0.22670
5.	C	-0.218231	0.37312
6.	C	0.193832	0.56037
7.	F	-0.124984	-0.30913
8.	F	-0.180342	-0.30183

9.	C	-0.909218	0.26528
10.	N	-0.146025	-0.22959
11.	F	-0.180342	-0.30183
12.	F	-0.124984	-0.30913

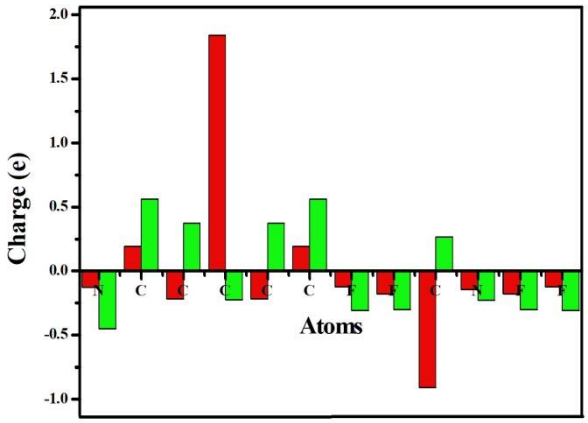

Figure 4: Mulliken atomic and natural charge graph of 2356TF4PC molecule

All carbon atoms are negative charged, while the carbon atoms (C2, C6) connected to the N1 nitrogen atom in the pyridine ring exhibit positive charge. The C4 carbon atom attached to the pyridine ring exhibit positive charge because of the influence of cyano group in the compound. Among these, the C4 carbon atom exhibit highest positive charge (1.8413 e) and C9 carbon atom shows highest negative charge (-0.9092 e). All the fluorine atoms and nitrogen atoms in the compound exhibit negative charges.

3.6 Vibration Analysis

The DFT/B3LYP approach was used to calculate the vibrational frequencies for the optimal molecular structure of the molecule. The 2356TFPC molecule's optimised molecular structure exhibits C1 point group symmetry. The molecule has 12 atoms and 30 fundamental normal vibrational modes, all of which are planar. The symmetry species of all vibrational modes is the same. Figures (5) and (6) show the combined theoretical and experimental FT-IR and FT-Raman spectra, respectively. Table (5) shows the computed and experimental wavenumbers, as well as their assignments. To determine

the greatest likelihood of vibrations, vibrational assignments of 2356TFPC with potential energy distribution (PED) have been presented.

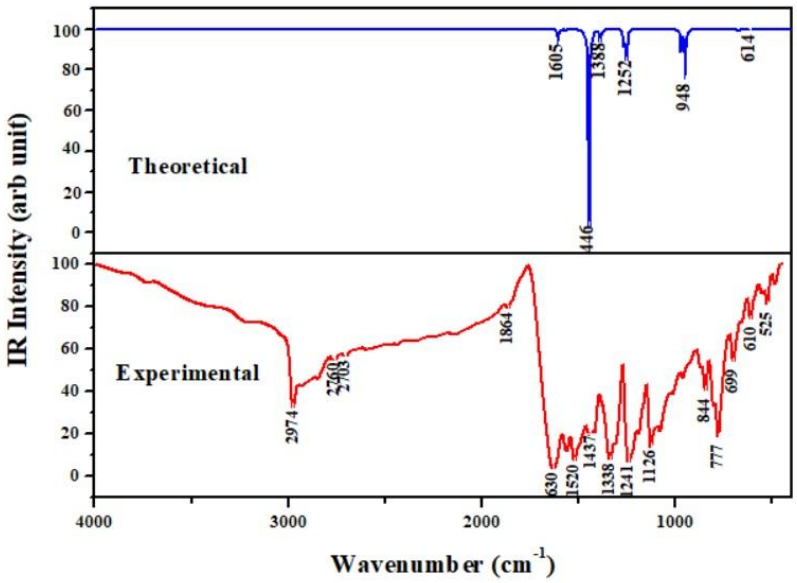

Figure 5: Combined FT-IR spectrum of 2356TF4PC molecule

3.6.1 C-C vibration

The C–C stretching pyridine ring of an aromatic ring is depicted in the same frequency range as the C–C stretching pyridine ring and it is commonly occurred in the region 1635-1100cm^{-1} [30]. The vibrational frequencies theoretically computed at 1605, 1433, and 1265 cm^{-1} in the 2356TFPC molecule are assigned to C–C stretching vibration. C–C stretching vibrations are ascribed to the band seen at 1630, 1445 and 1240 cm^{-1} in the infrared spectrum and 1649, 1436 and 1225 cm^{-1} in the Raman spectra. The C-C stretching vibration that appeared at 1265 cm^{-1} had the largest PED contribution of 78 percent, whereas the C-C stretching vibration that occurred in the remaining regions had low PED contributions of 67 percent, and 20 percent. The experimental data differs somewhat from the estimated values, and this difference is due to side chain elements. C-C in plane bending vibration and C-C out of plane bending vibration are both commonly observed in the 700-400 cm^{-1} range [31]. Theoretically C-C in plane bending vibration observed at 437 cm^{-1} with 62 percent PED contribution.

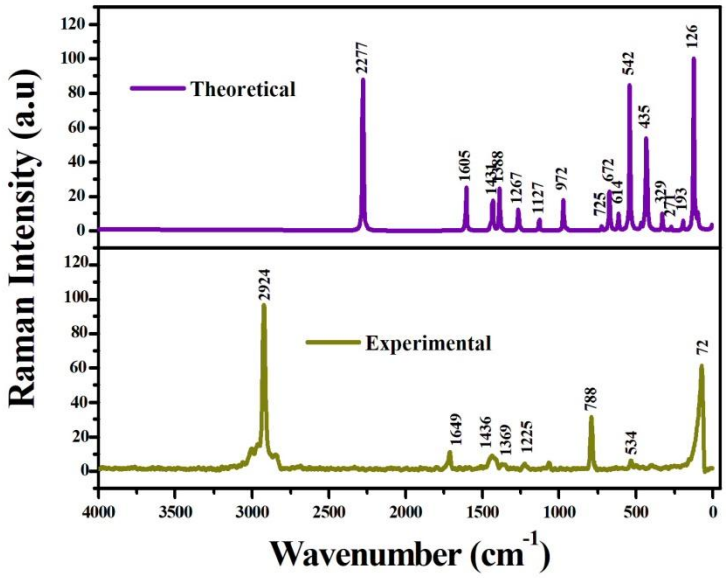

Figure 6: Combined FT-Raman spectrum of 2356TF4PC molecule

3.6.2 C-N and C≡N vibration

Aromatic ring C-N stretching bands are generally detected in the same frequency range of 1450-950cm^{-1} [32]. The C-N stretching in FT-IR spectra occurs as a strong peak in the region 1326 cm^{-1} in the current investigation. The region 1369 cm^{-1} in FT-Raman have a very weak peak. The theoretically analysed C-N vibration occur at the region 1386 cm^{-1}, with PED contributions of 83 percent. The C≡N stretching mode is seen in the 2210–2270cm^{-1} range [33]. Theoretically calculated C≡N stretching mode is observed in the region 2280 cm^{-1} with 89 percent PED contribution.

3.6.3 C-F vibration

Stretching bands in aromatic fluorine compounds range from 1270 to 1100 cm^{-1} [34,35]. Theoretically calculated C-F stretching vibrations occurs in the region 1466, 1251, 1128, 971 and 948 cm^{-1} with highest PED contribution of 78 percent in 1128 cm^{-1}. The stretching of the carbon–fluorine bond was seen in the infrared spectrum in the range of 1124 and 982 cm^{-1}. The large range is caused by the stretching frequency's sensitivity to other substituents in the molecule. With more than one fluorine atom, monofluorinated compounds have a strong band between 1000 and 1110 cm^{-1} that breaks into two, one for the symmetric mode and the other for the asymmetric mode. Because the carbon–fluorine bands are so strong, any carbon–hydrogen bands that may be present may be suppressed [36]. The vibrations of nearby atoms or groups are easily altered.

Table 5: Comparison of experimental wavenumbers (cm^{-1}) and computational (scaled) wavenumbers (cm^{-1}) of 2,3,5,6 Tetrafluoro-4-pyridine carbonitrile molecule using density functional theory method.

Wave numbers			Assignments with PED (>10%)
Experimental values		Scaled values	
FT-IR	FT-Raman		
--	--	2280	$\upsilon N_{10}C_9$ (89)
1630	1649	1605	υC_5C_6 (67) + $\beta C_3C_2N_1$ (11)
1520	--	1568	υN_1C_6 (67)
--	--	1466	υF_7C_2 (81) + $\beta C_2N_1C_6$ (10)
1437	1436	1433	υC_4C_9(20) + $\beta C_3C_2N_1$ (11) + $\beta C_5C_6N_1$ (18)
1338	1369	1386	υN_1C_2 (83)
1241	1225	1265	υC_2C_3 (78)
1126	--	1251	$\upsilon F_{11}C_5$ (61) + $\beta C_3C_2N_1$ (11)
--	--	1128	υF_8C_3 (78)
982	--	971	$\upsilon F_{12}C_6$ (60)
--	--	948	$\upsilon F_{11}C_5$ (73)
777	788	729	$\gamma C_9C_3C_5C_4$ (84)
--	--	725	$\beta C_2C_3F_8$ (85)
699	--	675	υF_7C_2 (20) + $\beta C_3C_2N_1$ (48)
--	--	674	$\gamma F_7C_3N_1C_2$ (98)
610	--	615	$\tau N_{10}C_9C_4C_3$ (11) + $\tau C_2N_{10}C_6C_5$ (84)
525	534	541	υC_4C_9 (48) + υC_2C_3 (15) + $\beta C_2N_1C_6$ (22)
498 --	-- --	468 437	$\beta C_4C_9N_{10}$ (64) υC_2C_3 (11) + $\beta C_2C_3C_4$ (62)
--	--	436	$\gamma F_7C_3N_1C_2$ (98)
--	--	431	$\beta C_4C_9N_{10}$ (71)
--	--	425	$\tau N_{10}C_9C_4C_3$ (56) + $\gamma C_9C_3C_5C_4$ (28)
--	--	329	$\beta C_2N_1C_6$ (76)
--	--	296	$\beta C_6C_5F_{11}$ (82)
--	--	289	$\tau N_{10}C_9C_4C_3$ (12) + $\tau C_4C_3C_2N_1$ (67) + $\tau C_2N_1C_6C_5$ (15)
--	--	272	$\beta C_6C_5F_{11}$ (76) + $\beta C_5C_6N_1$ (12)
--	--	195	$\gamma C_9C_3C_5C_4$ (90)
--	--	125	$\beta C_4C_9N_{10}$ (85)

--	--	110	$\tau C_3C_2N_1C_6$ (99)
--	72	99	$\tau N_{10}C_9C_4C_3$ (15) + $\gamma F_{11}C_4C_6C_5$ (22) + $\gamma F_8C_2C_4C_3$ (51)

3.7 AIM Analysis:

Atoms In Molecules (AIM) is a novel method created by R. Bader, which claims that the electron density ρ(r) is a local function of the molecular system. The atoms in molecule quantum theory (AIM) is a valuable technique for determining π-π interactions and hydrogen bonding within a molecule. This method is commonly used to calculate inter-atomic and intra-atomic interactions. Multiwfn (3.7) software program was used to do the topology analysis. Local minima (3, +3) also known as Cage Critical Point (CCP), local maxima (3, -3) also known as Nuclear Critical Point (NCP), first-order saddle point (3, +1) also known as Ring Critical Point (RCP), and second-order saddle point (3, -1) also represented as Bond Critical Point (BCP) are the four types of non-degenerate stable critical points (CPs) of rank 3 that correspond to the configurations of nuclei, bonds, and rings. The topology of the total electron density (ρ(r)), the Laplacian of electron density ($\nabla^2\rho(r)$) at the bond critical point, the potential energy density that defines the system to focus electrons at BCPs, and the local kinetic energy densities that signifies the electron potential to expand out in space can all be used to define the chemical insights of atoms, molecules, structures, and bonds [37-40]. The ellipticity of interacting atoms or fragments determined is indicated in Table (), and the molecular surface map for 2356TF4PC is shown in Fig (7). The strong hydrogen interactions are expressed by the large values of $\nabla^2\rho(r)$ and ρ(r). The electron density ρ(r) is essential in values where $\nabla^2\rho(r)$ is negative, and it also displays the charge concentration in the internuclear region. A strong covalent nature is shown by the negative sign of $\nabla^2\rho(r)$ at the binding of critical point (CP). Positive Laplacian values, on the other hand, are linked to charge weakening in the internuclear region. All the total electron density ρ(r) values are positive whereas Laplacian of electron density $\nabla^2\rho(r)$ are negative except the critical points between C-F bonds.

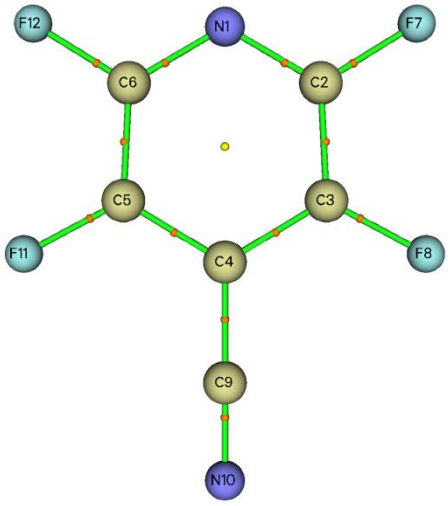

Figure 7: Structure of 2356TF4PC molecule with critical points

Table 6:Topological Parameters:Electron density (ρ), Laplacian of Electron density ∇2ρ),Ellipticity at Bond Critical point (BCP).

Name	Atoms	ρ	$\nabla^2 \rho$	Ellipticity
BCP1	N_1-C_2	0.3602	-1.0376	0.2541
BCP2	C_2-C_3	0.3186	-0.9109	0.3685
BCP3	C_3-C_4	0.3081	-0.8535	0.3011
BCP4	C_4-C_5	0.3081	-0.8535	0.3011
BCP5	C_5-C_6	0.3186	-0.9109	0.3685
BCP6	C_6-N_1	0.3602	-0.1038	0.2541
BCP7	C_2-F_7	0.2721	0.0563	0.0359
BCP8	C_3-F_8	0.2684	0.1540	0.0209
BCP9	C_4-C_9	0.2814	-0.7693	0.0660
BCP10	C_9-N_{10}	0.4789	-0.2161	0.0256
BCP11	C_5-F_{11}	0.2684	0.1540	0.0209
BCP12	C_6-F_{12}	0.2721	0.0563	0.0359

3.8 ELF and LOL Analysis:

Edgecombe and Becke developed the electron localisation function (ELF) for Hartree–Fock (HF) calculations in 1990, and Schmider and Becke extended it to density functional theory (DFT) in 2000. The electron localization function (ELF) analysis is used to better comprehend and define the chemical structure and chemical bonding of our molecule Because the reduction of the quantum kinetic-energy density by orbital sharing is the driving force of covalent bonding, the kinetic-energy

density acts as the primary attribute on which the localization descriptors are formed. ELF provides a local measure of Pauli repulsion that is directly related to electron kinetic energy. The larger the ELF [0.0 to 1.0] value, the more localised electrons are, indicating the presence of a covalent link, inner shells, or a lone pair of atoms, whereas the smaller values (0.5) represent regions where electrons are predicted to be delocalized [41-43]. In Fig (8a, b), the colour shaded map and relief map of ELF and LOL are depicted, with the relief map delineating the electron environment around each atom with large or contracted peak areas. Because they are based on kinetic energy density, ELF and LOL have a chemical component that is similar. The electron pair density is explained by ELF, but the maximum localised orbitals overlapping owing to orbital gradient is explained by LOL [44]. ELF has a range of values from 0.0 to 1.0, with larger values between 0.5 and 1.0 indicating regions with bonding and nonbonding localised electrons, and smaller values (0.5) indicating regions where electrons are predicted to be delocalized. A large value within this region indicates a high localization of electrons due to the presence of a covalent bond (a lone pair of electrons) or a nuclear shell in that region. The delocalized electron cloud around a few carbon atoms is depicted by the blue areas around them.

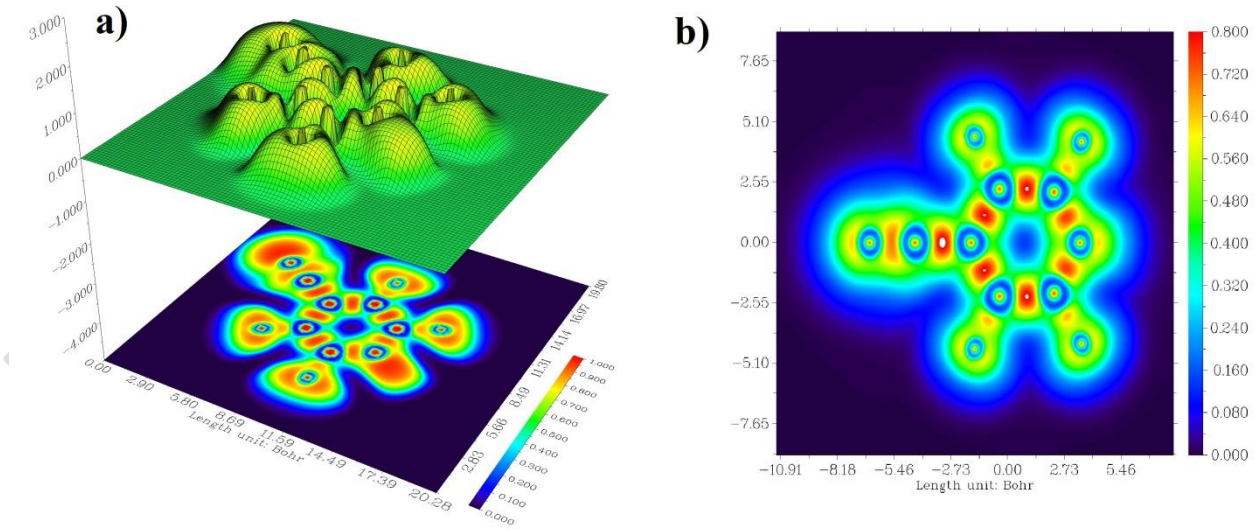

Figure 8 a: ELF relief map of 2356TF4PC molecule, b: LOL colour filled map of 2356TF4PC molecule

3.9 RDG Analysis:

Topology analysis was used to explain the electrical and chemical properties of 2356TF4PC. DFT/B3LYP/6-311++G(d,p) generated the Gaussian output, which was then used in the Multiwfn (3.7)

software for topology analysis. RDG is an extension of AIM analysis that is used to explain non-covalent weak interactions [45]. The weak interactions of 2356TF4PC have a strong relationship with the electron density. In general, the region with small ρ is for Van der Waals interaction, whereas 2356TF4PC regions have a substantial steric influence and hydrogen bond regions. Figure (9a, b) shows the reduced density gradient structure and scatter graph of 2356TF4PC compound. The spikes in the Reduced density gradient graphic show significant negative sign($\lambda_2\rho$) values, i.e. (sign($\lambda_2\rho$)<0), which suggests hydrogen bonding interactions, and high positive sign($\lambda_2\rho$) values, i.e. (sign($\lambda_2\rho$)>0), which indicates steric effect (strong repulsion), which is a non-bonding interaction. And when sign($\lambda_2\rho$) is virtually zero, i.e. (sign($\lambda_2\rho$)=0), it suggests a very weak interaction, i.e. Vander Waals interaction. The negative sign of ((λ_2)*ρ) refers to H-bond (weak bond) strong attractive interaction in the blue circle area. The green circle indicates a region with low electron density, which corresponds to the Van der Waals interaction. The steric effect is depicted in red to illustrate the most repulsive interaction. The core of pyridine ring indicates a significant steric influence represented in red coloured region. The RDG scatter graph shows strong hydrogen bond interaction and a strong repulsive interaction.

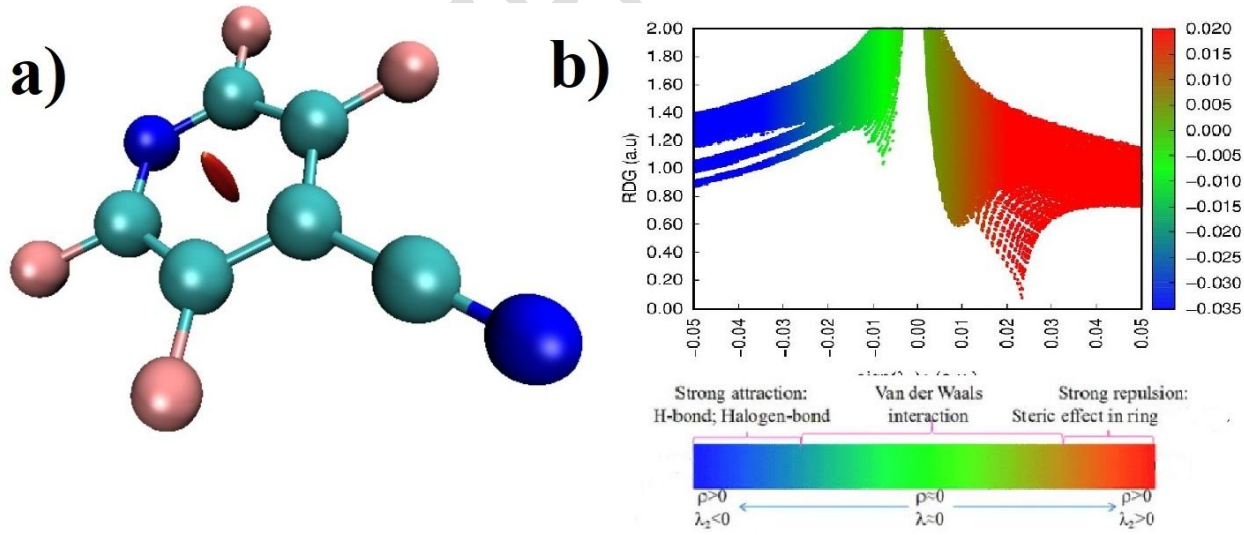

Figure 9 a: RDG structure of 2356TF4PC molecule, b: Scatter plot RDG versus the electron density ρ multiplied by the sign of λ2

3.10 Fukui Function

The electrophilic and nucleophilic nature of each atom in a molecule can be calculated using Fukui function. It is based on population analysis and they are quantitative information of each atom like. It is the method of adding or removing an electron from the molecule. From this analysis the

reactivity of 2356TF4PC is obtained using multiwfn program. A molecule's reactivity and selectivity can be studied using DFT method. Chemical potential, hardness, and softness are global qualities associated with chemical reactivity, whereas selectivity is associated with local reactivity. The Fukui function is the most essential local reactivity parameter. The Fukui function provides information on a molecule's highly electrophilic and nucleophilic core. The preferred regions where a chemical species (molecule) will amend its density when the number of electrons is changed, or the tendency of the electronic density to deform at a given position when accepting or donating electrons, are indicated by the local reactivity descriptors like the Fukui function [46,47]. Fukui function can be calculated for three different conditions such as nucleophilic f^+, electrophilic f^-, and radial f^o attack and dual descriptors.

$$\text{Nucleophilic attack, } f^+(r) = q_r(N+1) - q_r(N)$$

$$\text{Electrophilic attack, } f^-(r) = q_r(N) - q_r(N-1)$$

$$\text{Radial attack, } f^o(r) = [q_r(N+1) - q_r(N-1)]/2$$

$$\text{Dual descriptor, } \Delta f(r) = f^+(r) - f^-(r)$$

where q_r corresponds to atomic charge evaluated from mulliken charge, N corresponds to atomic charge, (N+1) corresponds to cationic state and (N-1) corresponds to anionic state [48-50]. Regions in chemical species with the highest values of the Fukui function (fj) demonstrate significant reactivity for comparable attacks, according to Parr and Yang et.al., (1984) [50]. The Fukui functions derived from the NBO charges have been reported to be satisfactory. The nucleophilic, electrophilic and radical attack of the compound is shown in fig (10 a, b, c). Fukui functions including nucleophilic, electrophilic and dual descriptors of the selected compound is represented in table (7). From the dual descriptor, the nucleophilic site ($\Delta F>0$) for the compound is C9 which has a positive value, while the electrophilic sites ($\Delta F<0$) for the compound in the descending order is N10>N1>C4>F7>F12>F8>F11>C3>C5>C2>C6. The selected compound shows much electrophilic sites when compared to nucleophilic attack. This shows that the selected compound has much biological activity and can be used in designing new medicines for diseases.

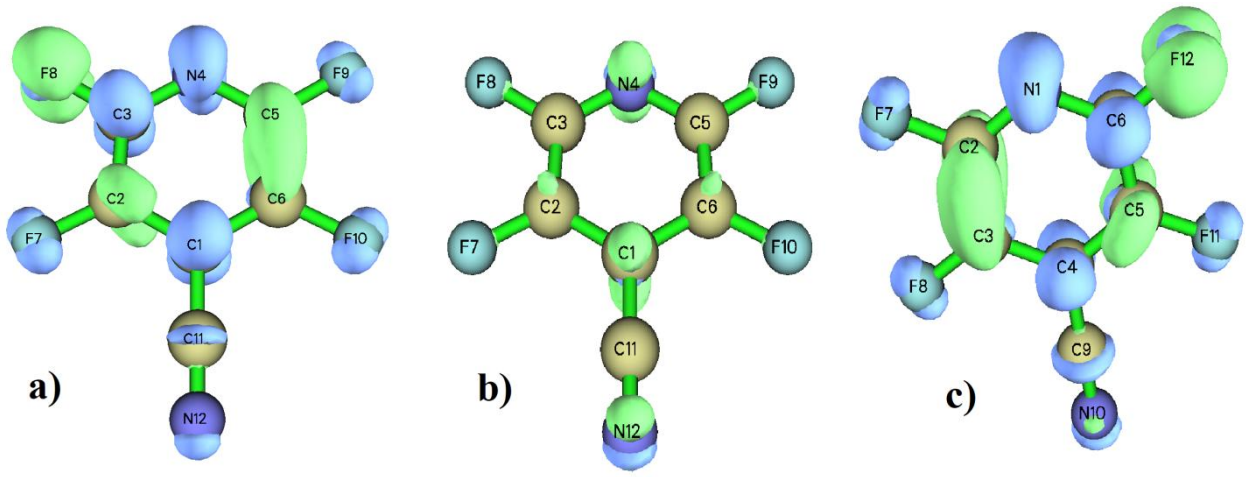

Figure 10 a: Electrophilic attack in 2356TF4PC molecule, b: Nucleophilic attack in 2356TF4PC molecule, c: Radial attack in 2356TF4PC molecule

Table 7: Using Mulliken population analysis: Fukui functions (f_j+,f_j-, f_j0, f(r)) for atoms of 2,3,5,6 Tetrafluoro-4-pyridine carbonitrile molecule using density functional theory method.

Atoms	Mulliken atomic charge			Fukui function			
	N	N+1	N-1	f+	f-	f^o	Δf
N1	-0.1266	-0.2917	-0.0229	-0.1651	0.1037	-0.1344	-0.2688
C2	-0.1938	0.1724	0.2605	0.3662	0.4543	-0.04405	-0.0881
C3	-0.2182	-0.3141	-0.1523	-0.0959	0.0659	-0.0809	-0.1618
C4	-1.8413	1.6969	1.9098	3.5382	3.7511	-0.1065	-0.213
C5	-0.2182	-0.3141	-0.1523	-0.0959	0.0659	-0.0809	-0.1618
C6	0.1938	0.1724	0.2606	-0.0214	0.0668	-0.0441	-0.0882
F7	-0.1249	-0.1876	-0.0065	-0.0627	0.1184	-0.0905	-0.181
F8	-0.1803	-0.2441	-0.0701	-0.0638	0.1102	-0.087	-0.174
C9	-0.9092	-0.9032	-0.9437	0.006	-0.0345	0.0203	0.0405
N10	-0.1460	-0.3552	-0.0064	-0.2092	0.1396	-0.1744	-0.3480
F11	-0.1803	-0.2441	-0.0701	-0.0638	0.1102	-0.087	-0.174
F12	-0.1250	-0.1876	-0.0065	-0.0626	0.1185	-0.0905	-0.1811

3.11 Molecular docking studies

Molecular docking is an important tool in structure-based drug design that can help to simplify and accelerate medication development. Scientists could use molecular docking to screen the

interaction between the ligand and the target protein, along with predict the binding conformations and affinities of any species to the target protein. The recent discovery of a novel coronavirus poses a threat to public health around the world, prompting the World Health Organization to proclaim it a global pandemic. However, no specific pharmacological treatment for Cov-19 has yet been developed [51]. In order to find a new medication, we conducted computational study of the molecule within the coronavirus active site and four other activity proteins to see how it interacts. All five selected proteins' pdb files were retrieved from the RCSB protein database. The selected proteins are inflammatory, SARS Cov2, fungal, malarial, cancer and their pdb id's are (3n8y, 6cs2, 1ks5, 1j3i and 1qh4). All bonded waters and biomolecules were manually removed from the protein, Geisteger and Kollman charges were calculated, and polar hydrogen atoms were inserted using Autodock software. The protein ligand interaction of five different proteins is shown if figure 11 (a-e) and the binding affinity of the ligand with the protein is presented in table (8). The 2356TFPC molecule interacted deeply with 3n8y, making three hydrogen bonds with the amino acids TYR371, SER516, and MET508, with a binding affinity of 7.1 kcal/mol. The nitrite N_{10} atom forms 3.14 Å and 3.20 Å bonds with the TYR371 and SER516 residues, respectively. The pyridine nitrogen N_1 atom formed a hydrogen bond with the MET508 residue over a distance of 2.77 Å, with a binding affinity of 5.33 kcal/mol. Second, the 2356TFPC molecule formed a hydrogen bond with the protein 6cs2, with a binding energy of 6.2 kcal/mol. At 2.0 Å bond distance, the nitrogen atom in the pyridine ring makes a hydrogen bond with the residue THR760. Third, the ligand 2356TFPC was docked with the protein 1ks5, making a hydrogen bond with the amino acids GLU116, resulting in a binding score of 5.3 kcal/mol. At a distance of 3.30 Å, oxygen in GLU116 interacts with nitrogen in the pyridine ring. Fourth, the ligand 2356TFPC was docked with the protein 1j3i, where it formed two hydrogen bonds with the amino acids SER108 and VAL45 yielding a binding score of 6.0 kcal/mol. SER108's oxygen binds with nitrogen in the pyridine ring at a distance of 2.94 Å, while nitrogen in the pyridine ring interacts with oxygen in VAL45 at a distance of 2.04 Å. The ligand 2356TFPC was docked with the protein 1qh4, making two hydrogen bonds with the amino acids LEU209 and ASP54, resulting in a binding score of 6.1 kcal/mol and. The oxygen in LEU209 binds to nitrogen N_1 in the pyridine ring at a distance of 3.11 Å, while the oxygen in ASP54 bonds to nitrogen N_1 at a distance of 3.35 Å. MEP analysis revealed that the ligand's electrophilic and nucleophilic sites were suitable for hydrogen bonding interaction

with the chosen protein target. The complete protein ligand complex exhibits hydrogen bonding with the ligand's reactive region [52].

Table 8:Molecular docking of 2,3,5,6 Tetrafluoro-4-pyridine carbonitrile molecule against different protein targets.

Protein (PDB:ID)	Binding residues	Bond distances (Å)	Binding energy (kcal/mol)
3n8y	TYR-371	3.14	-7.1
	SER-516	3.20	
	MET-508	2.77	
6cs2	THR-760	2.0	-6.2
1ks5	GLU-116	3.3	-5.3
1j3i	SER-108	2.94	-6.0
	VAL-45	2.04	
1qh4	LEU-209	3.11	-6.1
	ASP-54	3.35	

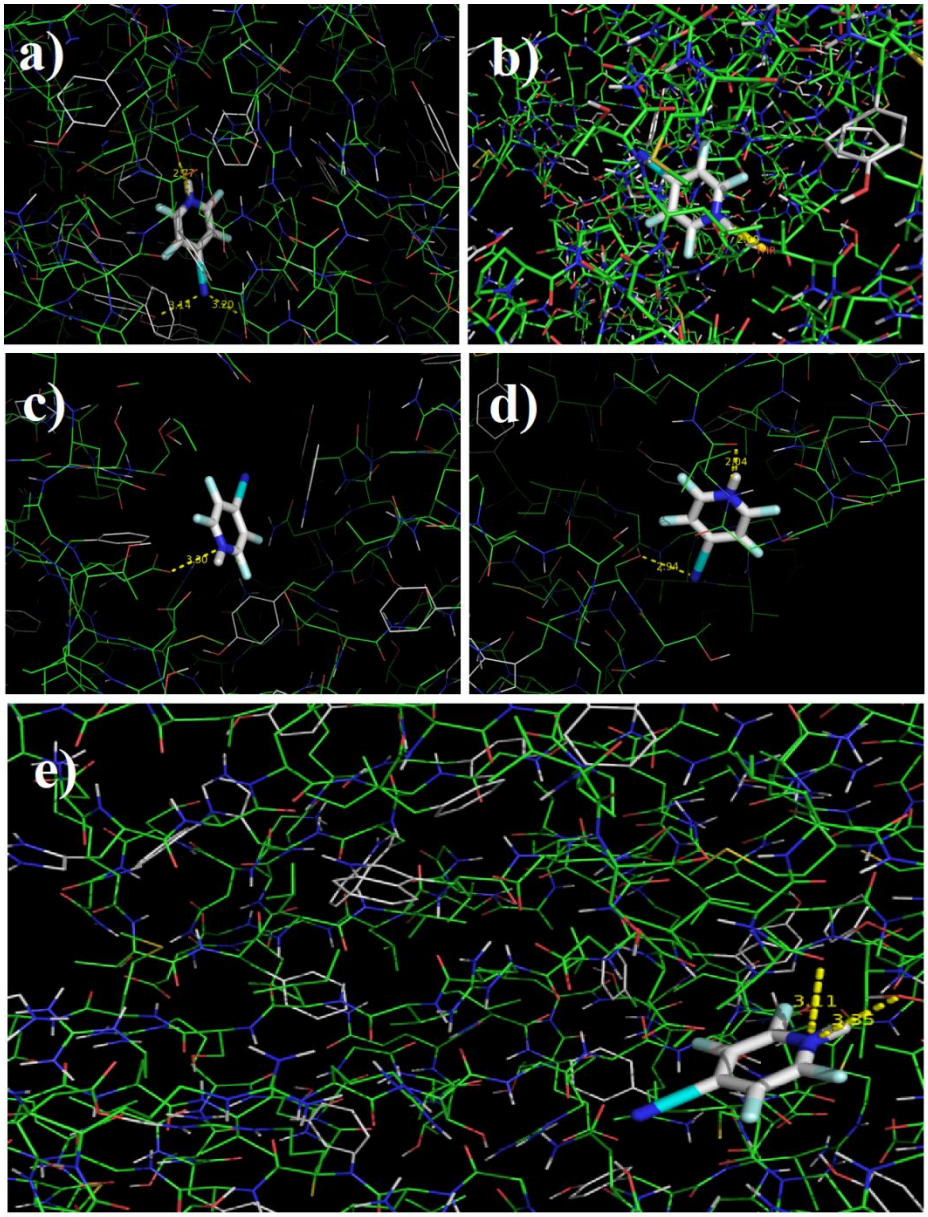

Figure 11 a: Ligand docked with inflammatory protein, b: Ligand docked with SARS Cov2 protein, c: Ligand docked with fungal protein, d: Ligand docked with malarial protein, e: Ligand docked with cancer protein

4. Conclusion

Using the DFT / B3LYP / 6-311 ++ G (d, p) basis set, the optimal geometry and vibrational wave numbers of the title chemical 2356TFPC were calculated. The vibrational spectra were assigned PED calculations using VEDA software. The molecule's stability is demonstrated by the strong intramolecular hyper-conjugative interaction between the lone pair and the anti-bonding

orbital. The experimental IR and Raman data were compared to the vibrational modes. The simulated experimental and theoretical spectra were found to be in good agreement. The Mulliken Population method and natural population analysis were used to calculate the net charge distribution of title chemical. Negative potential sites and positive potential sites are found according to the MEP analysis. The ionisation potential, hardness, electronegativity, electrophilicity index, electron affinity, and chemical potential can all be estimated semi-quantitatively using the derived HOMO and LUMO energies. The Fukui function aids in determining the electrophilic and nucleophilic properties of a molecule's particular location. According to the stability of the molecule to softness, the molecule with the smallest energy gap is the most reactive molecule. The molecular docking analysis was carried out for more well-known targeted proteins such as SARS Cov2, inflammatory, fungal, malarial, and cancer proteins, and the docking results reveal that the targeted compound has stronger anti-inflammatory activity with high binding affinity than other active proteins.

Reference

1. Premkumar S, Jawahar A, Mathavan T, et al. DFT calculation and vibrational spectroscopic studies of 2-(tert-butoxycarbonyl (Boc)-amino)-5-bromopyridine. Spectrochimica Acta Part A: Molecular and Biomolecular Spectroscopy. 2014;129:74-83.
2. Premkumar S, Rekha, TN, Rajkumar BJ, et al. Vibrational spectroscopic and structural investigations of 2-amino-6-methoxy-3-nitropyridine: a DFT approach. Brazilian Journal of Physics. 2015;45(6):621-632.
3. Krishnakumar V, Xavier RJ. Density functional theory calculations and vibrational spectra of 3, 5-dibromopyridine and 3, 5-dichloro-2, 4, 6-trifluoropyridine. Spectrochimica Acta Part A: Molecular and Biomolecular Spectroscopy. 2005;61(1-2):253-260.
4. Premkumar S, Jawahar, A, Mathavan T, et al. Vibrational spectroscopic and DFT calculation studies of 2-amino-7-bromo-5-oxo-[1] benzopyrano [2, 3-b] pyridine-3 carbonitrile. Spectrochimica Acta Part A: Molecular and Biomolecular Spectroscopy. 2015;138:252-263.

5. Medhi RN, Barman R, Medhi, KC, et al. Ultraviolet absorption and vibrational spectra of 2-fluoro-5-bromopyridine. Spectrochimica Acta Part A: Molecular and Biomolecular Spectroscopy. 2000;56(8):1523-1532.
6. Topacli A, Bayarı S. Normal coordinate analysis of 4-aminopyridine. Effect of substituent on pyridine ring in metal complexes of 4-substituted pyridines. Spectrochimica Acta Part A: Molecular and Biomolecular Spectroscopy. 2001;57(7):1385-1391.
7. Arjunan V, Isaac ASR, Rani T, et al. Density functional theory studies on vibrational and electronic spectra of 2-chloro-6-methoxypyridine. Spectrochimica Acta Part A: Molecular and Biomolecular Spectroscopy. 2011;78(5):1625-1632.
8. PiĢta E, Proniewicz E, Kudelski A, et al. Vibrational characterization of α-aminophosphinic acid derivatives of pyridine: DFT, Raman and SERS spectroscopy studies. Vibrational Spectroscopy. 2016;83:115-125.
9. Márquez MJ, Márquez MB, Cataldo PG, et al. A comparative study on the structural and vibrational properties of two potential antimicrobial and anticancer cyanopyridine derivatives. Open Journal of Synthesis Theory and Applications. 2015;4(01):1.
10. Waly MA, EL-Hawary II, Hamama WS, et al. Synthesis and antitumor evaluation of some new fused and binary pyridines. Journal of Heterocyclic Chemistry. 2013;50(S1):E12-E17.
11. Amr AEGE, Abdel-Hafez NA, Mohamed SF, et al. Synthesis, reactions, and antiarrhythmic activities of some novel pyrimidines and pyridines fused with thiophene moiety. Turkish Journal of Chemistry. 2009;33(3):421-432.
12. Gholap AR, Toti KS, Shirazi F, Kumari R, et al. Synthesis and evaluation of antifungal properties of a series of the novel 2-amino-5-oxo-4-phenyl-5, 6, 7, 8-tetrahydroquinoline-3-carbonitrile and its analogues. Bioorganic & medicinal chemistry. 2007;15(21):6705-6715.
13. Frisch M J. et al., Gaussian 09 Revision D.01, Gaussian Inc., Wallingford, CT, 2009..
14. Schlegel HB., Optimization of equilibrium geometries and transition structures. Journal of Computational Chemistry. 1982: 3:214–218.
15. Frisch A, Nielson AB, Holder AJ, GAUSSVIEW User Manual, Gaussian Inc, Pittsburgh, PA, 2000.
16. Jamroz MH, Vibrational Enegy Distribution Analysis, VEDA 4 Computer Program, Poland, 2004.

17. Scott AP, Random L, Harmonic Vibrational Frequencies: An Evaluation of Hartree−Fock, Møller−Plesset, Quadratic Configuration Interaction, Density Functional Theory, and Semiempirical Scale Factors. Journal of Physical Chemistry. 1996: 100: 16502- 16513.
18. Keresztury G, Chalmers JM, Griffith PR, Raman Spectroscopy: Theory in Handbook of Vibrational Spectroscopy, vol. 1, John Wiley & Sons Ltd, New York, 2002.
19. Glendening ED, Reed AE, Carpenter JE, Weinhold F. NBO Version 3.1, TCI, University of Wisconsin, Madison, 1998.
20. Snehalatha M, Ravikumar C, Joe IH, et al. Spectroscopic analysis and DFT calculations of a food additive Carmoisine. Spectrochimica Acta Part A: Molecular and Biomolecular Spectroscopy. 2009;72(3):654-662.
21. Schwenke DW, Truhlar DG, Systematic study of basis set superposition errors in the calculated interaction energy of two HF molecules. The Journal of chemical physics 1985;82(5):2418-2426.
22. Chattaraj PK, Roy DR, Giri S, et al. An atom counting and electrophilicity based QSTR approach. Journal of Chemical Sciences. 2007;119(5):475-488.
23. Fan WJ, Zhang RQ, Liu, S. Computation of large systems with an economic basis set: Structures and reactivity indices of nucleic acid base pairs from density functional theory. Journal of computational chemistry. 2007;28(5):967-974.
24. Mumit MA, Pal TK, Alam MA, et al. DFT studies on vibrational and electronic spectra, HOMO–LUMO, MEP, HOMA, NBO and molecular docking analysis of benzyl-3-N-(2, 4, 5-trimethoxyphenylmethylene) hydrazinecarbodithioate. Journal of molecular structure. 2020;1220:128715.
25. Okulik N, Jubert AH. Theoretical analysis of the reactive sites of non-steroidal anti-inflammatory drugs. Internet Electronic Journal of Molecular Design. 2005;4(1):17-30.
26. Politzer P, Laurence PR, Jayasuriya K. Molecular electrostatic potentials: an effective tool for the elucidation of biochemical phenomena. Environmental health perspectives. 1985;61:191-202.
27. Mulliken RS. Electronic population analysis on LCAO–MO molecular wave functions. I. The Journal of Chemical Physics. 1955;23(10):1833-1840.

28. Danie VA, Kumari BJ, Nirmal NF, et al. Molecular structure, vibrational assignment, HOMO-LUMO and mulliken analysis of 2-(4-amino-2-phenylaminothiazol-5-oyl)-N-methylbenzimidazole by DFT method. 2014;2:21-24.
29. Amalanathan M, Rastogi VK, Joe IH, et al. Density functional theory calculations and vibrational spectral analysis of 3, 5-(dinitrobenzoic acid). Spectrochimica Acta Part A: Molecular and Biomolecular Spectroscopy. 2011;78(5):1437-1444.
30. Kandasamy M, Velraj G. Ab initio/DFT electronic structure calculations, spectroscopic studies of 5-bromo-2-pyridinecarbonitrile–A comparative study. Solid state sciences. 2012;14(8):1071-1079.
31. Subashchandrabose S, Babu NR, Saleem H, et al. Vibrational studies on (E)-1-((pyridine-2-yl) methylene) semicarbazide using experimental and theoretical method. Journal of Molecular Structure. 2015;1094:254-263.
32. Colthup NB, Daly LH, Wiberley SE. "Introduction to Infrared and Raman Spectroscopy", Academic Press, New York. 1990.
33. Sert Y, Sreenivasa S, Doğan H, et al. Vibrational frequency analysis, FT-IR and Laser-Raman spectra, DFT studies on ethyl (2E)-2-cyano-3-(4-methoxyphenyl)-acrylate. Spectrochimica Acta Part A: Molecular and Biomolecular Spectroscopy. 2014;130:96-104.
34. Krishnakumar V, Sangeetha R, Mathammal R, et al. Density functional theory, comparative vibrational spectroscopic studies, HOMO–LUMO, first hyperpolarizability analyses of 2-fluoro 5-nitrotoluene and 2-bromo 5-nitrotoluene. Spectrochimica Acta Part A: Molecular and Biomolecular Spectroscopy. 2013;104:77-86.
35. Ushakumari L, Varghese HT, Panicker CY, et al. Vibrational spectroscopic studies and DFT calculations of 4-fluoro-N-(2-hydroxy-4-nitrophenyl) benzamide. Journal of Raman Spectroscopy: An International Journal for Original Work in all Aspects of Raman Spectroscopy, Including Higher Order Processes, and also Brillouin and Rayleigh Scattering. 2008;39(12):1832-1839.
36. Socrates G. Infrared and Raman characteristic group frequencies: tables and charts. John Wiley & Sons. 2004.

37. Janani S, Rajagopal H, Muthu S, et al. Molecular structure, spectroscopic (FT-IR, FT-Raman, NMR), HOMO-LUMO, chemical reactivity, AIM, ELF, LOL and Molecular docking studies on 1-Benzyl-4-(N-Boc-amino) piperidine. Journal of Molecular Structure. 2021;1230:129657.
38. Bader RFW, Austen MA. Properties of atoms in molecules: atoms under pressure. The Journal of chemical physics. 1997;107(11):4271-4285.
39. Popelier PLA, Aicken FM, O'Brien SE. Atoms in molecules (p. 132). Manchester: Prentice Hall.2000.
40. Noureddine O, Gatfaoui S, Brandan SA, et al. Experimental and DFT studies on the molecular structure, spectroscopic properties, and molecular docking of 4-phenylpiperazine-1-ium dihydrogen phosphate. Journal of Molecular Structure. 2020;1207:127762.
41. Clements RJ, Womack JC, Skylaris CK. Electron localisation descriptors in ONETEP: a tool for interpreting localisation and bonding in large-scale DFT calculations. Electronic Structure 2020;2(2):027001.
42. Bitter T, Ruedenberg K, Schwarz WHE. Toward a physical understanding of electron-sharing two-center bonds. I. General aspects. Journal of computational chemistry. 2007;28(1):411-422.
43. Ruedenberg K, Schmidt MW. Why does electron sharing lead to covalent bonding? A variational analysis. Journal of computational chemistry. 2007;28(1):391-410.
44. Silvi B, Savin A. Classification of chemical bonds based on topological analysis of electron localization functions. Nature 1994;371(6499):683-686, https://doi.org/10.1038/371683a0.
45. Lu T, Manzetti S. Wavefunction and reactivity study of benzo [a] pyrene diol epoxide and its enantiomeric forms. Structural Chemistry. 2014;25(5):1521-1533.
46. Ayers PW, Parr RG. Variational principles for describing chemical reactions: the Fukui function and chemical hardness revisited. Journal of the American Chemical Society. 2000;122(9):2010-2018.
47. Parr RG, Yang W. Density functional approach to the frontier-electron theory of chemical reactivity. Journal of the American Chemical Society. 1984;106(14):4049-4050.
48. Fathima Rizwana B, Prasana JC. et al. Spectroscopic investigation (FT-IR, FT-Raman, UV, NMR), Computational analysis (DFT method) and Molecular docking studies on 2-[(acetyloxy)

methyl]-4-(2-amino-9h-purin-9-yl) butyl acetate. International Journal of Materials Science. 2017;12(2):2017.

49. Sánchez-Márquez J. Correlations between Fukui indices and reactivity descriptors based on Sanderson's principle. The Journal of Physical Chemistry A. 2019;123(40), 8571-8582.
50. Renuga S, Karthikesan M, Muthu S. FTIR and Raman spectra, electronic spectra and normal coordinate analysis of N, N-dimethyl-3-phenyl-3-pyridin-2-yl-propan-1-amine by DFT method. Spectrochimica Acta Part A: Molecular and Biomolecular Spectroscopy. 2014;127:439-453.
51. Abraham CS, Muthu S, Prasana JC, et al. Computational evaluation of the reactivity and pharmaceutical potential of an organic amine: A DFT, molecular dynamics simulations and molecular docking approach. Spectrochimica Acta Part A: Molecular and Biomolecular Spectroscopy. 2019;222:117188.
52. Robert HM, Usha D, Amalanathan M, et al. Spectroscopic (IR, Raman, UV, NMR) characterization and investigation of reactive properties of pyrazine-2-carboxamide by anti-bacterial, anti-mycobacterial, Fukui function, molecular docking and DFT calculations. Chemical Data Collections. 2020;30:100583.